Sandia National Laboratories

Operated for the United States Department of Energy
by National Technology and Engineering Solutions
of Sandia, LLC.

Albuquerque, New Mexico 87185-0101
Livermore, California 94551-0969

date: *March 2, 2023*

to: Sandia National Laboratory WIPP Records Center

from: Paul S. Domski and Martin Nemer, SNL WIPP Geochemistry

subject: On the Occurrence and Solubility of the Magnesium Hydroxy-Chloride Phases: Phase 3 and Phase 5 in the WIPP Near-Field Environment

Introduction

The objective of this document is to address the Environmental Protection Agencies (EPA) Issue 7 (Peake, 2022), regarding Phase 5 solubility. In this memo we compare the solubility of Phase 3 and Phase 5, as implemented in the WIPP thermodynamic database (DATA0.FM1)[1] and those calculated by Nemer and Domski (2023), to measured laboratory solubilities and discuss the potential for occurrence of these phases in the WIPP environment.

Phase 3 and Phase 5 are categorized as magnesium oxy-chloride phases ($Mg_kCl_l(OH)_m \cdot nH_2O$). Understanding the occurrence and solubility of magnesium oxy-chloride phases, also known as Sorel cement phases, is important in the WIPP near-field environment. The presence of the MgO engineered barrier and prevalence of sodium-chloride and sodium-magnesium-chloride brines in the WIPP near-field renders an environment conducive to the formation of magnesium oxy-chloride phases. In the WIPP post-closure environment the MgO will hydrate to form brucite ($Mg(OH)_2$(s)) which will react with carbon dioxide from the microbial degradation of the cellulose, plastic, and rubber (CPR) materials in the waste to form hydromagnesite ($Mg_5(CO_3)_4(OH)_2.4H_2O$) (Brush et al., 2012). The equilibrium that is established between brucite and hydromagnesite buffers the pH of the system around pH 9 while also maintaining a very low fugacity of carbon dioxide; both conditions which are favorable to maintain actinide solubility at low levels. In this environment, magnesium oxy-chloride phases are known to form (Altmaier et al. 2002, Xiong et al. 2009, and Pannach et al. 2017). The two phases of interest to the WIPP are $Mg_2Cl(OH)_3.4H_2O$, known as 3-1-8 in the engineering literature[2] (Pannach et al. 2017), or as Phase 3, and $Mg_3Cl(OH)_5.4H_2O$ known as 5-1-8 in the engineering literature also known as Phase 5. Phase 5 has been observed in WIPP laboratory experiments dealing with the hydration of the MgO engineered barrier (Xiong and Lord, 2008 and Deng et al., 2009), and it may play an important role in the water balance within the repository.

The findings indicate that the continued use of $Mg(OH)_2 – MgCl_2 – H_2O$ model as currently implemented in the WIPP thermodynamic database is sufficient. Furthermore, it is the authors' recommendation that

[1] The solubility constants of Phase 3 and Phase 5 included in DATA0.FM1 are the same values included in DATA0.FM4.
[2] This designation arises from the whole number of Mg-hydroxides, Mg-chlorides, and water molecules, i.e., $3Mg(OH)_2$ $MgCl_2$ $8H_2O$ = 3-1-8, required to form the phase, and in this case representing two unit cells.

Exceptional Service in the National Interest
This article has been authored by an employee of National Technology & Engineering Solutions of Sandia, LLC under Contract No. DE-NA0003525 with the U.S. Department of Energy (DOE). The employee owns all right, title and interest in and to the article and is solely responsible for its contents. The United States Government retains and the publisher, by accepting the article for publication, acknowledges that the United States Government retains a non-exclusive, paid-up, irrevocable, world-wide license to publish or reproduce the published form of this article or allow others to do so, for United States Government purposes. The DOE will provide public access to these results of federally sponsored research in accordance with the DOE Public Access Plan https://www.energy.gov/downloads/doe-public-access-plan.
Sandia National Laboratories
U.S. DEPARTMENT OF ENERGY NNSA

Phase 5 be suppressed in future recertification analyses until additional experimental data suggests otherwise.

Note that the chemical conditions of the experiments and the simulations of the experiments included in this memo are representative of simplified WIPP systems and are not representative of the chemical conditions expected in the near-field environment after the WIPP brines react with the MgO engineered barrier, waste containers, and their contents. For example, the equilibrium near-field brine compositions predicted for CRA-2019 (Domski and Sisk-Scott, 2019) include potassium, calcium, iron, lead, sulfate, borate, and bromine none of which are included in the experiments reviewed in this memo. Furthermore, the brucite – hydromagnesite buffer reaction credited with maintaining pH values of ≈ 9 and low $pCO_2(g)$ ≈ 2 x 10^{-6} atm expected in the WIPP near-field is not directly addressed in the experiments. A comprehensive evaluation of pertinent magnesium oxy-chloride phase literature is provided below.

Altmaier et al. (2003)

Altmaier et al. (2003) studied the solubility of crystalline brucite in NaCl (0.1 – 5.6 m), $MgCl_2$ (0.01 – 2.7 m) solutions, and mixtures of 0.5 and 5.0 m NaCl containing 0.01 – 0.05 m $MgCl_2$ at 22 ± 2 °C. Altmaier et al. (2003) observed that in $MgCl_2$ solutions above 2.0 m brucite converted to Phase 3. Phase 3 solubility was studied in 2.1 – 5.2 m $MgCl_2$ solutions. Using the Pitzer parameters of Harvie et al. (1984), Altmaier et al. (2003) calculated the log K values of brucite (17.1 ± 0.2) and Phase 3 (26.0 ± 0.2) confirming those of Harvie et al. (1984), and, thus, DATA0.FM1 which implements Harvie et al.'s values.

Altmaier et al. (2003) also observed the conversion of brucite to Phase 3 with no other magnesium oxychloride phases, such as Phase 5 observed.

> *"Moreover there are no indications of the presence of other magnesium oxychloride hydrate phases like $Mg_3(OH)_5Cl{\cdot}4H_2O(cr)$. Scanning electron microscopy (SEM) coupled with energy-dispersive spectrometry (EDS) showed needle-like crystals with a length of 10–100 µm and confirmed the element ratio of Mg:Cl:O = 2:1:7."*

Figure 1 shows the Table 3 measured solubility data of Altmaier et al. (2003) for brucite and Phase 3 in $MgCl_2$ solutions plotted with the EQ3/6 simulated data using the Harvie et al. (1984) log K and Pitzer parameters as implemented in DATA0.FM1. This figure reproduces Figure 5 in Altmaier et al. (2003) except for the Phase 5 simulation plotted here. All the WIPP thermodynamic databases from DATA0.FM1 through the current database, DATA0.FM5, use the same Pitzer parameters and log K values for brucite and Phase 3 as Harvie et al. (1984), i.e. the same as used by Altmaier et al. (2003). The Phase 5 simulation plotted in Figure 1 was included to illustrate the similarity between the measured Phase 3 data, the Phase 3 simulation, and the Phase 5 simulation. Based on Figure 1 it could be argued that both the Phase 3 and Phase 5 simulations fit the measured Phase 3 data equally well. From a simulation standpoint the occurrence of these two phases is nearly indistinguishable, and if the uncertainty in their log K values and Pitzer parameters were taken into consideration, phase stability via a thermodynamic model would likely be unidentifiable.

Figure 1 also shows that the model predicts that as the concentration of Mg increases from mMg = 0. 0 m the phase stability goes from Brucite to Phase 5 at mMg = 1.5 m, and from Phase 5 to Phase 3 at mMg = 2.3 m. In other words, Phase 5 is only stable for $1.5 \leq m\text{Mg} \leq 2.3$, but as quoted above Altmaier et al. (2003) did not observe Phase 5 in their experiments as the model predicts. Note that the experiments of Altmaier et al. (2003) were not in the model-predicted range of Mg concentration where Phase 5 is expected to occur, which may explain why it was not observed. Additionally, Pannach et al. (2017)

observed that Phase 5 converts to Phase 3 over time periods of ~60 days at 298 °K and ~20 days at 313 °K.

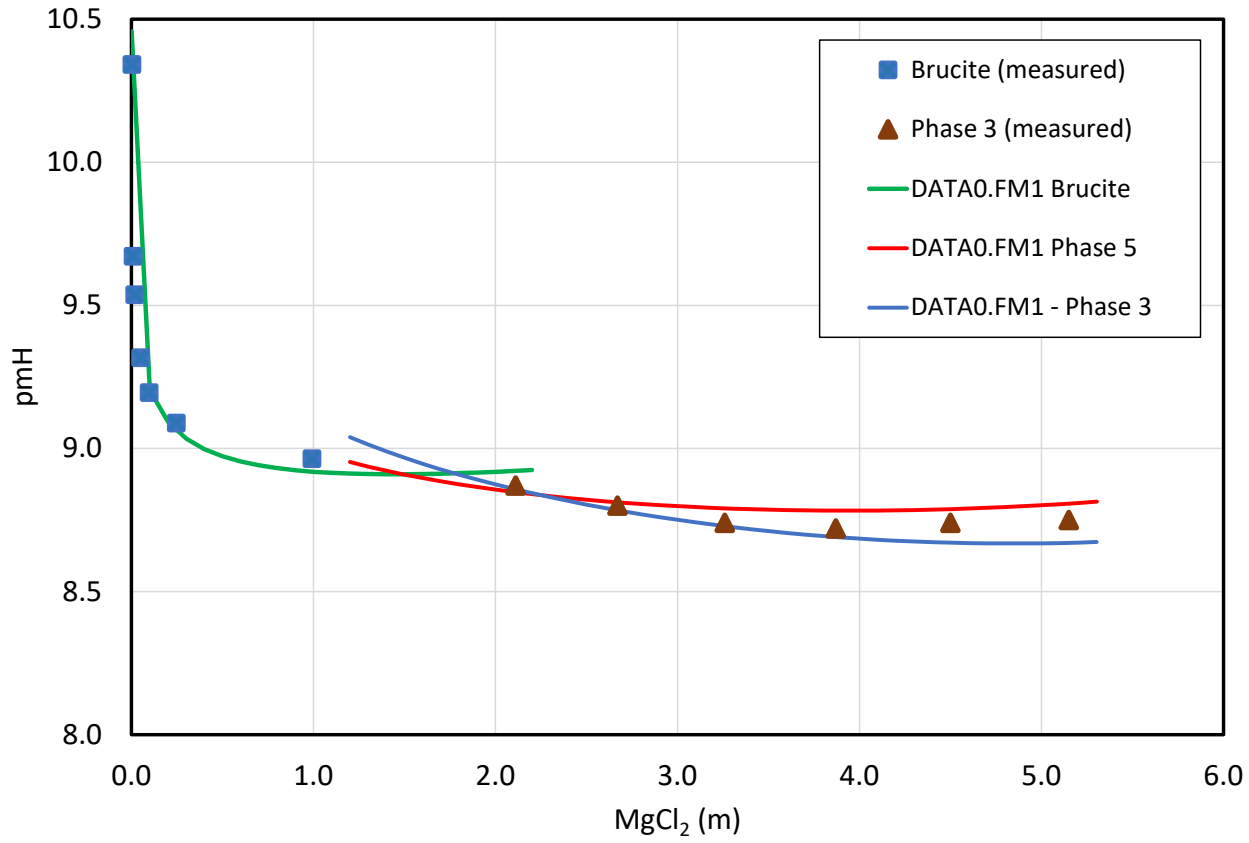

Figure 1. Altmaier et al. (2003) brucite and Phase 3 data in $MgCl_2$ solutions compared to the modeled brucite and Phase 3 solubilities using the log K values and Pitzer parameters of Harvie et al. (1984) and Phase 5 log K value from Xiong et al. (2010). All files stored at: cvs/CVSLIB/WIPP_EXTERNAL_phase5memo.

Nemer and Domski (2023) provides alternate fits to the data of Altmaier et al. (2003), which alters the stability fields for both phases plotted in Figure 1.

In summary, the results of Altmaier et al. (2003) are consistent with the Harvie et al. (1984) log K values for Brucite (17.1) and Phase 3 (26.0) and with the observation of no other magnesium oxy-chloride phases form at the magnesium concentrations used in the experiments.

Pannach et al. (2017)

Pannach et al. (2017) studied the solubility of Sorel cement phases in $MgCl_2$ solutions at temperatures ranging from 298 to 393 °K. The goals of this study were to collect solubility data and identify the stable magnesium oxychloride phases as a function of temperature and $MgCl_2$ concentration. For the purposes of the WIPP we are currently only concerned with the data and results collected at 298 K which are in alignment with the WIPP chemical conditions conceptual model (Wilson et al., 1996).

Table 2 in Pannach et al. (2017) provides the measured data for the initial and final (equilibrium) systems, including the mass of the solid added to the initial solution at 298 K. The $MgCl_2$ concentration of the initial solutions range from 0.5 to 5.5 m in increments of 0.5 m with replicates for most concentrations.

Rather than providing the pH, or pmH of the experimental systems, Pannach provided the $Mg(OH)_2$ molality which is their expression of the OH^- concentration of the solution. Because Pannach et al. (2017) express the solubility of Phase 3 in terms of $Mg(OH)_2$ they posed the following:

> *"The determination of the OH^- solution concentration according to the dissolution reaction of basic magnesium chloride hydrates (e.g., reaction 3) is a more direct way to quantify the solubility equilibria.*
>
> *$3Mg(OH)_2{\cdot}MgCl_2{\cdot}8H_2O = 4Mg^{2+} + 6OH^- + 2Cl^- + 8H_2O$ (3)"*

Pannach et al. (2017) does not provide the solubility product of any of the magnesium oxychloride phases observed in their experiments, however at the end of the paper they state that it will be done in future work.

The following passage from Pannach et al. (2017) summarizes how the OH- concentrations were measured.

> *"The decrease in OH- concentrations in these solutions (from 0.5 to 5.0 mol $MgCl_2$ kg^{-1}) was monitored by a pH electrode over 37-105 days. The electrode potential was recorded regularly during aging of the solutions and correlated to that measured in n mol kg-1 $MgCl_2$ reference solutions with precisely known OH- concentration; hence, the OH- concentration could be derived directly from the measured potentials. An uncertainty of ±0.05 mol OH- resulted from a potential drift of ±3 mV during the time of data recording."*

For both undersaturation and oversaturation experiments at 298 K Pannach et al. (2017) note that brucite is the stable phase up to 1.5 m $MgCl_2$, with its solubility increasing with increasing $MgCl_2$ concentration. At $MgCl_2$ concentrations greater than 1.5 m Phase 3 becomes the stable phase.

Pannach et al. (2017) reports that for their oversaturation experiments at 298 K the first solid forms within the first 6 hours with an accompanying drop in the OH- concentration. This phase was identified after 50 hours by x-ray diffraction (XRD) as Phase 5, and at 63 days a slight drop in the OH- concentration marked the transformation of Phase 5 to Phase 3, and after 75 days the solid phase consisted of a mixture of Phase 5 and Phase 3. At slightly higher temperatures, 313 K, the same behavior was observed with complete transformation of Phase 5 to Phase 3 after 24 days. These observations agree with those of Urwongse and Sorrell (1980) for magnesia cement pastes, "*...the reaction proceeds by rapid formation of 5.1.8, which reaches a maximum in ≈ 25 h. The 3.1-8 forms more slowly, at the expense of 5.1.8, and becomes the major phase after ≈ 3 days.*"

In their undersaturation saturation experiments Pannach et al. (2017) did not observe Phase 5 at all, i.e., only Phase 3 was observed. However, it should be noted that Phase 3 was used as the starting material, and solids characterization for their undersaturation experiments was only performed at the termination of the experiments at 3 years. It is possible that Phase 5 may have existed for a time early in the experiment but was not observed. Note that the Mg concentration was increased in steps of ≈ 0.5 m in the Pannach experiments, which could have missed the Phase 5 stability field based on the simulations in Figure 1.

Pannach et al. (2017) questioned the quality of their measured solubility data at 298 K from over- and undersaturation, and ultimately decided the over saturation was systematically biased. The measured OH- concentration from the oversaturation experiments was consistently ≈ 7.5 x 10^{-4} m greater than that from undersaturation. Pannach attributed this offset in the oversaturation OH- concentrations to micro defects in the Phase 3[3] crystalline structure which would yield a higher solubility to this "meta" phase, thus, they discount the oversaturation data as nonrepresentative of Phase 3 solubility and support the undersaturation data. This offset in the OH- concentration is diminished at 313 K, and not observed at T>313 K, *"which implicates that either structural disorder of the 3-1-8 phase does not occur at elevated temperatures (>313 K), that the defects are degraded during the equilibrium period, or that the contribution of these defects to the phase solubility is negligible."* (Pannach et al, 2017).

Simulations of the Pannach et al. (2017) data were performed using EQ3/6. The initial solutions were set up in EQ3NR as 1.5 m $MgCl_2$ solutions at pmH = 8.0[4], which was the initial $MgCl_2$ concentration of their Phase 3 solubility experiments, the pmH was set in EQ3NR in the subsequent EQ6 simulations the code calculated the pH. The EQ6 simulation used the pickup file from EQ3NR and titrated Mg^{2+} and Cl^- as the reactant type "aqueous species", with Cl^- titrated at a relative rate twice that of Mg^{2+} to maintain electroneutrality. Phase 3 was titrated into solution as "pure mineral" with its relative reaction set to 100x of the Mg^{2+}, and 50x Cl^-. The purpose of the high reaction rate was to force Phase 3 saturation in the first reaction step while allowing Phase 3 to dissolve/precipitate as $MgCl_2$ concentration of the solution increased. The total OH^- of the system was calculated by taking the total of the molal concentrations of the aqueous species $MgOH^+$ and OH^- from the EQ6 reaction path output. The OH- values calculated in this manner were compared to the OH- calculated by multiplying the moles of dissolved Phase 3 by 3 (there are 3 moles OH^-/mole Phase 3) and nearly identical results were obtained. The slight difference in the OH- concentrations can be accounted by the dissociation of water, which the Phase 3 budget method did not include. The total Mg concentration from the EQ6 simulations include both the Mg^{2+} aqueous species titrant, and that from the dissolution of Phase 3. Note, that inspection of the EQ6 output confirmed that Phase 3 maintained a saturation index of zero throughout the reaction path.

The undersaturation Phase 3 solubility data collected by Pannach at 298 K are plotted in Figure 2 together with the EQ3/6 simulations for Phase 3 and Phase 5. While the Phase 3 simulated solubility does not visually appear to fit the measured Phase 3 data as well as the fit to the Altmaier et al. (2003) data (Figure 1) the Pannach Phase 3 data still supports the model. This is further explored in Nemer and Domski (2023), where an uncertainty analysis shows that despite the visual lack of fit, the Pannach data fits to a modified log K value within a 95'th percent credible interval on the posterior-predictive distribution. Because of that analysis, it is the authors' position that additional independent experimental evidence would be needed before doubting the Pannach data or the model. The Phase 5 simulation shown in Figure 2 deviates considerably from the measured data as well.

The cause of the discrepancy between the Pannach measurements and the simulated Phase 3 solubility may be related to the log β and the binary Pitzer parameters for the aqueous species $MgOH^+$, and the $MgOH^+/Cl^-$ pair, respectively. Preliminary trial and error visual fitting of these parameters (not included in this memo) compared to the measurements revealed that both the shape and slope of the simulated response is affected by changing these parameters.

[3] Pannach et al. (2017) used both XRD and SEM for post-test phase identification.
[4] The effect of the starting EQ3NR pmH value was tested and shown to not impact the pmH of the subsequent EQ6 run.

In summary, the Pannach et al. (2017) study showed that at 298 K: 1) Brucite was stable in $MgCl_2$ solutions up to 1.5 m before transforming to Phase 3 (Altmaier saw this transformation at 2 m); 2) Phase 5 forms early in the oversaturation experiments but is metastable and transforms to Phase 3 over short time frames of ~60 days at 298 K, and ~20 days at 313 K; and 3) the measured Phase 3 data of Pannach supports the WIPP Phase 3 model. It should be noted that for both the Altmaier and Pannach experiments the increment of change in the Mg concentration was large relative to the predicted stability field for Phase 5, therefore, it is possible that these experiments may have been insensitive to Phase 5 formation.

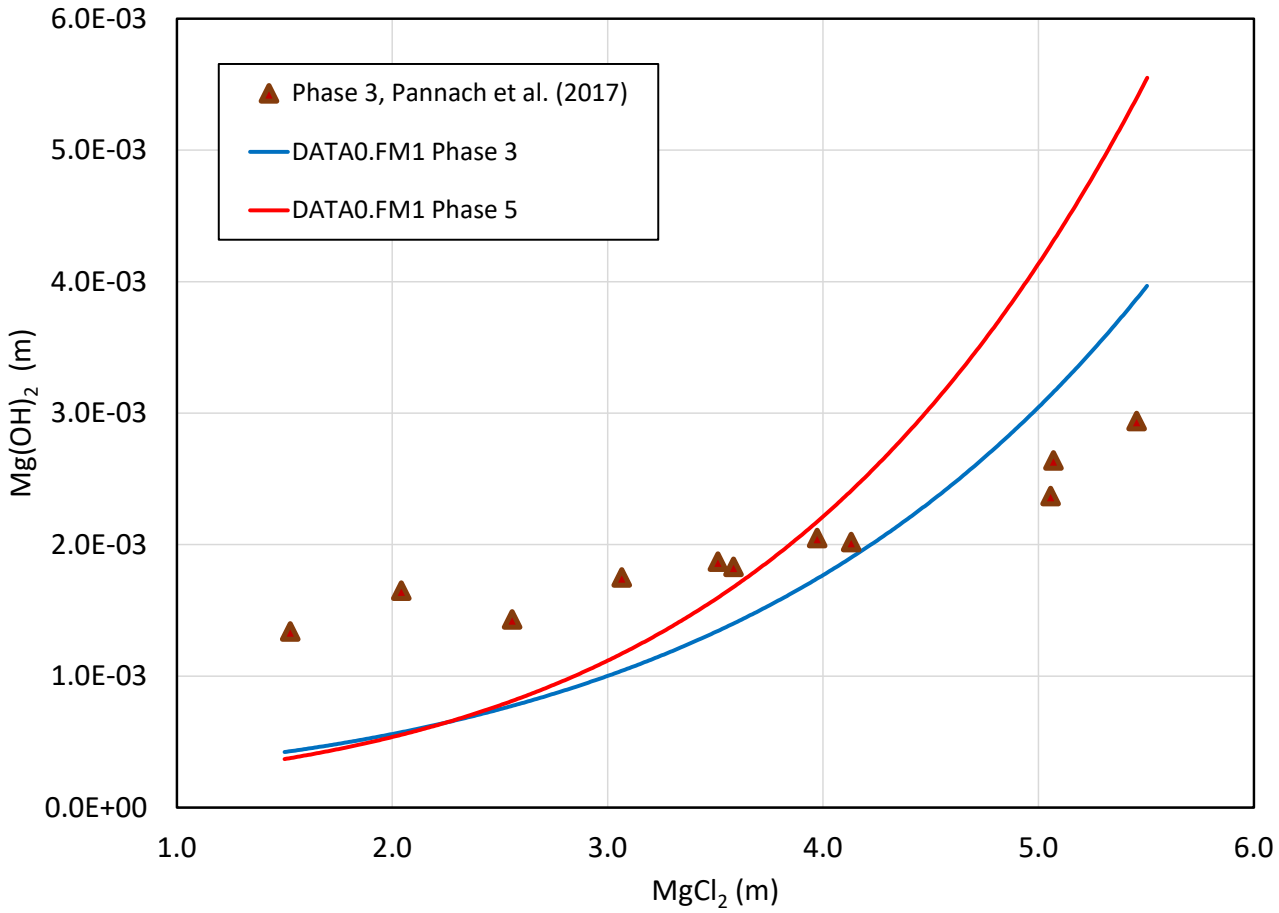

Figure 2. Pannach et al. (2017), Phase 3 measured data in $MgCl_2$ solutions plotted with the EQ3/6 simulated Phase 3 and Phase 5 solubilities using the log K values and Pitzer parameters of Harvie et al. (1984), DATA0.FM1. All files stored at: cvs/CVSLIB/WIPP_EXTERNAL_phase5memo.

Xiong and Lord (2008)

Xiong and Lord (2008) executed a series of experiments to determine the reaction path in the MgO – CO_2 – H_2O system where they varied the matrix solution composition, the partial pressure of CO_2(g), the Mg reactant, whether the solution was stirred or static, and if the CO_2(g) was bubbled or passively dissolved in solution. Xiong and Lord (2008) examined 20 permutations/scenarios of the above variables; the full experimental matrix is presented in Table A-1 of Appendix A. The solid materials were periodically collected from each of the reactors for a period up to about 4 years, solution properties such as pH and constituent concentrations were not measured. The solid materials were characterized using X-ray diffraction (XRD) methods and the evolution of the solids are presented in a series of figures showing the

XRD traces as a function of sample age. Xiong and Lord (2008) identified the presence of Phase 5 in experiments which examined the carbonation of MgO in WIPP GWB brine at ambient temperature (22.5 ± 1.5 °C) and atmospheric CO_2(g) partial pressure ($p_{CO2} = 10^{-3.4}$).

Five of the twenty reactors were set up using GWB as the matrix solution. Two of these reactors were static (i.e. not stirred) with CO_2(g) in passive (i.e. not bubbled) equilibrium with the solution. These were the only two reactors where Phase 5 was observed to have formed. The only difference between the two reactors where Phase 5 was observed was the choice of Mg reactant; in one reactor Premier MgO (periclase) was used, and in the other $Mg(OH)_2$(s) (brucite) was used as the reactant. The X-ray diffraction patterns for these two reactors are shown in Fig. 4 of Xiong and Lord (2008) for the periclase reactant, and Fig. 12 of Xiong and Lord (2008) for the brucite reactant. The periclase reactor showed brucite, calcite, halite, periclase, and Phase 5 in its XRD trace (Fig. 4, Xiong and Lord, 2008). The brucite reactor had hydromagnesite, brucite, halite, and Phase 5 present in its XRD trace (Fig. 12, Xiong and Lord, 2008). The phases in these figures are denoted as the following: MC = Mg-oxychloride (Phase 5); B = brucite; C = calcite; P = periclase; H = hydromagnesite; and HA = halite.

Figures 4 and 12 of Xiong and Lord (2008) shows that the experiment with the periclase (Fig. 4) reactant had a much better developed Phase 5 XRD reflections, and that appear much earlier (50 days) compared to the experiment with brucite (Fig. 12) as the reactant where the XRD peaks are very small and don't appear until 368 days. The larger more well defined XRD reflections are an indication of the greater relative abundance of Phase 5 in the periclase experiment. A second observation from these two experiments is that hydromagnesite is not observed in the periclase experiment while it was observed in the brucite experiment. However, calcite occurs in the periclase experiment while it does not in the brucite experiment, essentially trading one carbonate phase for another with the source of calcium being the impurities noted by Xiong and Lord (2008) in the Premier MgO. Halite was observed in both the periclase and brucite experiments, as it was in seven of the other experimental setups, which could indicate that there were evaporative losses which would complicate interpretation of the observed phase assemblages.

In the memo by Xiong et al. (2009), in the introduction section it is stated that Phase 5 was observed in a solution comprised of 1.0 M $MgCl_2$ and 3.6 M NaCl using Martin Marietta MgO as the reactant. However, this author has not been able to trace this solution back to previous references, and until that is resolved this work will not be further considered.

Given the qualitative nature of the Xiong and Lord (2008) study it's not possible to draw any definite conclusions on the mode of occurrence of the phases observed in the experiments. For the current memo, the only observation that can be made is that Phase 5 was only observed to form in GWB brine; however, within the uncertainty of the experimental procedure (e.g. potential unaccounted evaporation) it would be premature to state that Phase 5 formation is exclusive to GWB brine. An additional observation regarding the GWB - periclase experiment is the occurrence of calcite and Phase 5 together, which is consistent with a simulation result in the CRA-2019 baseline solubility calculations (Domski and Sisk-Scott, 2019).

The results of Xiong and Lord (2008) are for conditions not expected for the WIPP near-field environment predicted in the baseline solubility model (Domski and Sisk-Scott, 2019). The results of Domski and Sisk-Scott (2019) are for a closed system with respect to CO_2(g) and the GWB and ERDA-6 brines had been reacted with halite, anhydrite, brucite, hydromagnesite, ferrous hydroxide, and PbO, while Xiong and Lord (2008) were for systems open to CO_2(g) with an end-member brine(s) reacted with a Mg-reactant. The final composition of these reacted brines (Domski and Sisk-Scott, 2019) differs significantly from their initial compositions, and likely from those of Xiong and Lord (2008), who did not analyze the

brine compositions, with higher pH of ≈ 9 and low $fCO_2 \approx 2 \times 10^{-6}$ atm, therefore, the reaction paths are expected to differ. Therefore, the results of Xiong and Lord (2008) may not be expected for the WIPP environment.

Deng et al. (2009)

Deng et al. (2009) investigated the long-term inundated hydration of MgO with the goal of determining the relative hydration kinetics. An experimental matrix was designed to test the hydration rate with three MgO particle sizes and two solid to liquid ratios in three WIPP-related brines (see Table 1, Deng et al. (2009) for the experimental matrix). The experiments were carried out in three WIPP brines, ERDA-6, GWB, and simplified GWB using Martin Marietta MgO in three particle sizes, "as-received MgO" which includes all particle sizes, and then the two particle sizes with the highest weight fraction, the large size at 1.0 – 2.0 mm, and the smaller size 75 μm. The two WIPP relevant MgO-to-brine ratios 3 g/11 mL, and 3.1g/77 mL were used in the experiments (see Deng et al. (2009) for explanation). Samples were sealed in serum bottles or centrifuge tubes and placed in 28 °C incubator for the duration of the experiments. Samples of solids and solution were collected periodically over the course of the experiment. With the pH and sample weight recorded the liquid fraction was analyzed using inductively coupled plasma atomic emission spectrometer (ICP-AES, Perkin Elmer DV 3300) to determine the concentration of dissolved Mg and Ca. Chloride concentration was measured using a Dionex 3000 ion chromatograph (IC). The solid material from the experiments was characterized using XRD, and the author notes *"…XRD is only used to identify the mineral phases present in the samples and not to quantify the amount of each phase."*. Solid characterization is presented as time-series of XRD traces in Deng et al. (2009) to observe the timing and development of the mineral phases for each set of experimental variables. Scanning electron microscopy (SEM) was also used to characterize solid materials.

The results of Deng et al. (2009) showed that for the ERDA-6 brine periclase hydrated to form brucite only. The timing of appearance of brucite in ERDA-6 was dependent of the particle size of the periclase with the brucite appearing first in the vessels with the smallest grain size, which correlates faster hydration times with increasing periclase surface area. In GWB the first hydration product to form is Phase 5 followed by brucite. This order of appearance is consistent with the other observations because Phase 5 is stable in higher concentrations of Mg, and as Phase 5 precipitates and the solution Mg concentration decreases, the stability field of brucite would be approached where an equilibrium would be established at the invariant point of these two phases. Similar to ERDA-6, hydration time of periclase was negatively correlated to particle size (i.e., positively correlated to grain surface area). In all cases, Phase 5 was observed for the 498-day duration of the experiment with no observed conversion to Phase 3. An observation worth noting is that compared to GWB, hydration of periclase in simplified GWB, which consists of 4.0 m NaCl and 1.0 m $MgCl_2$, is notably faster with much larger product peaks in the XRD traces, which qualitatively suggests more complete conversion of periclase to product phases. This observation suggests that some of the constituents of the complete GWB composition may be acting as inhibitors to the formation of periclase hydration products.

Deng et al. (2009) used EQ3/6 and log K value of Phase 5 provided by Xiong et al. (2009) to calculate the saturation index in their experiments. In all cases Deng et al. (2009) found that Phase 3 and Phase 5 were supersaturated in their experiments. This result is consistent with the Phase 5 model response observed in Figure 3 (see below) where the simulated Phase 5 solubility underpredicts the measured Mg concentrations. Deng et al. (2009) (Figure 30) also provided EQ3/6 simulations of the solubility of Phase 5 compared to their laboratory measured solubility with the same result, the simulated solubility shown in their Figure 30 was less than the measured solubility. It should be noted that in these experiments the

solution is in contact with 2-3 phases, periclase, brucite and Phase 5, therefore, the assumption of thermodynamic equilibrium may not be valid.

The important points from the Deng et al. (2009) for the purposes of this memo are as follows: 1) In GWB the hydration products of periclase follow the reaction path of Phase 5 followed by brucite precipitation; 2) periclase hydration in simplified GWB is rapid and more complete than observed in the full GWB composition brine, which suggests that the formation of hydration phases may be inhibited by a constituent(s) of the full GWB; 3) the simulated solubility using the log K value of Xiong et al. (2009) underpredicts the measured magnesium concentrations from the experiments, i. .e., the solubility predicted by the log K value of Xiong et al. (2009) is lower than the observed solubility.

Xiong et al. (2010)

Xiong et al. (2010) determined the log K value of Phase 5, from undersaturation in a series of solutions with variable NaCl and $MgCl_2$ concentrations (see Appendix A, Table A-2, for the experimental matrix). Two other studies on Phase 5 solubility were identified, Mazuranic et al. (1982) and Xia and Bao (1992). These studies were not considered in the current memo, Mazuranic et al. (1982) because they calculated "approximate solubility products", and Xia and Bao (1992) because an English translation of this work was not available.

Phase 5 was synthesized in the laboratory, and its pre-test identity confirmed using XRD. The experiments were conducted at room temperature (at 21 ± 1 °C) in 150 mL plastic bottles with 100 mL of matrix solution, and about 1 g of Phase 5 per bottle. The bottles were sealed with parafilm, placed in a water-bath shaker set at 140 rpm; apparently the experiments were not performed in a glove box, and therefore, CO_2(g) could potentially affect the results because of the initial exposure to atmospheric CO_2 and because parafilm may not form an impervious seal to the atmosphere.

The results of the experiments, the measured pH, calculated pmH, Mg (m), and Cl (m) are presented in Table 4 of Xiong et al. (2010). Also presented in Table 4 (Xiong et al., 2009 and 2010) are the Phase 5 solubility quotients and the Log K value for each set of measurements together with their average values. Xiong et al. (2010) extrapolated the log K values to zero ionic strength at 25 °C using the specific interaction theory (SIT) (43.21 ± 0.33), and the Pitzer model (42.96 ± 0.32). According to Xiong et al. (2010) *"There was no phase change after the experiments."*, however, no post-test XRD patterns are provided, and no discussion was provided regarding secondary phases that may have formed during the experiment as was observed in the same chemical system by Xiong and Lord (2008). Resolving this issue through additional experiments or examination of the records associated with the Xiong et al. (2010) is reserved for potential future work.

The Phase 5 Log K value derived using the Pitzer model was added to the WIPP thermodynamic database DATA0.FM1 (Xiong, 2011) and has been unchanged in all subsequent databases including DATA0.FM4 and DATA0.FM5.

The Environmental Protection Agency (EPA) requested in their Technical Support Document (TSD) (U.S. EPA, 2022) that the Department of Energy (DOE) demonstrate that "*the DATA0.FM4 database can be used to accurately model the experimental solubility data for Phase 5."*

Figure 3 shows the pmH versus the Mg (m) data from Table 4 of Xiong et al. (2010) and the EQ3/6 simulation using DATA0.FM1 of the experimental conditions. The model fit consistently underestimates the Mg concentration at a fixed pmH value. This comparison was not included in Xiong et al. (2010).

Xiong et al. (2010) does not provide a discussion regarding brucite and that it may be stable at Mg concentrations up to 1.5 m, or higher.

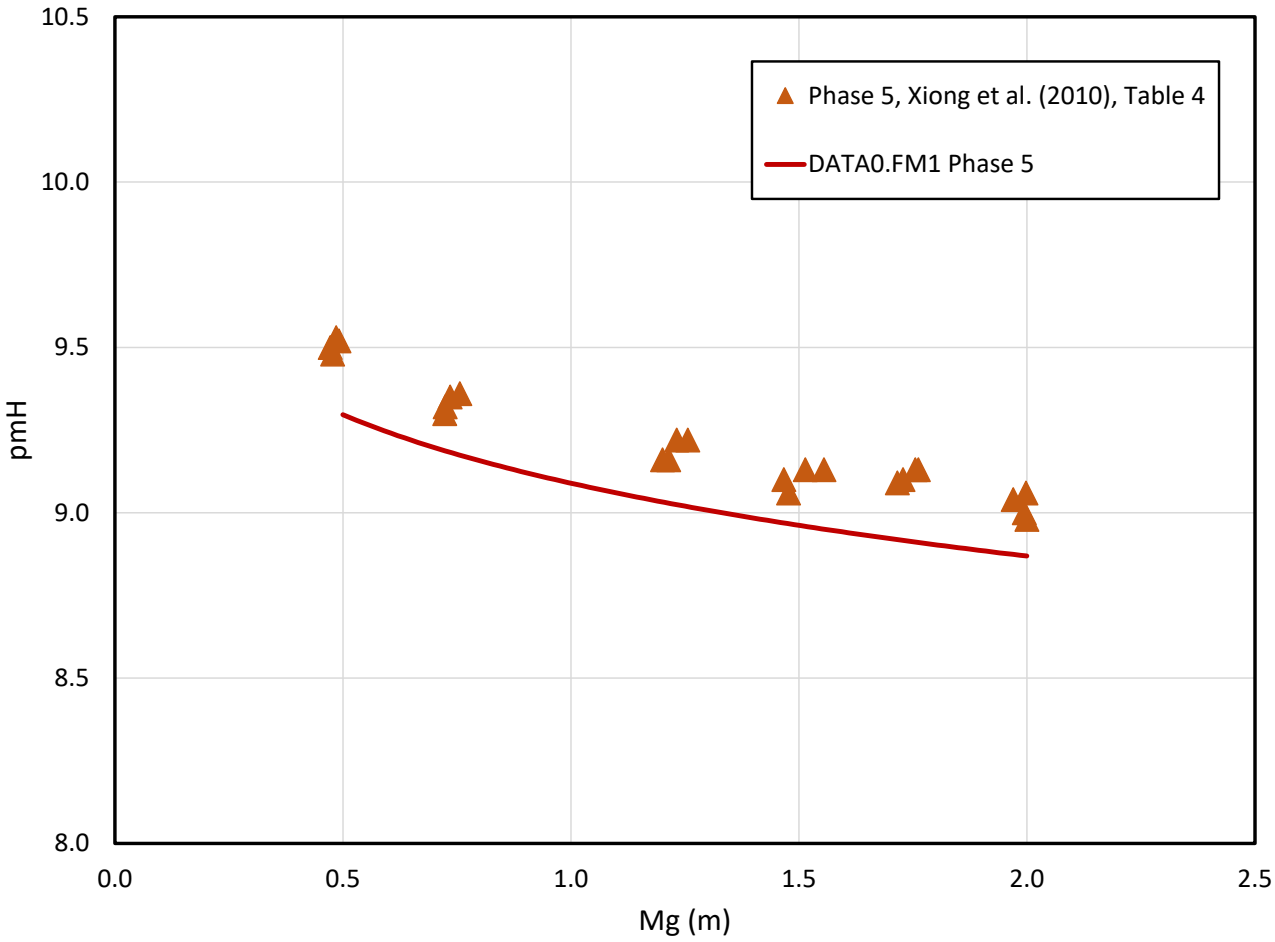

Figure 3. Xiong et al. (2010) Phase 5 solubility experiments measured magnesium and pmH data compared to the EQ3/6 simulation in mixed $MgCl_2$ – NaCl solutions. All files stored at: cvs/CVSLIB/WIPP_EXTERNAL_phase5memo.

In summary, Xiong et al. (2010) performed Phase 5 solubility experiments in the Na – Mg – Cl – H_2O system over a range of compositions (see Table A-2). From the measured solubility data, the log K value of Phase 5 was calculated for the SIT (43.21 ± 0.33), and the Pitzer model (42.96 ± 0.32), and the Gibb's free energy and enthalpy of formation were also derived. For the duration of the experiments, up to 4 years, Xiong et al. (2010) notes that there was no phase change, although no post-test XRD patterns are provided therefore, further experimental evidence is desired to confirm the experimental conclusions. Given that the reaction vessels were accessible to the atmosphere, it is possible that secondary carbonate phases might have formed as observed by Xiong and Lord (2008).

Comparison of the Harvie et al. (1984), Xiong et al. (2010), and Nemer and Domski (2023) Log K values

EQ3/6 runs were performed to investigate the solubility of Phase 3 and Phase 5 using the log K values derived by Harvie et al. (1984), Xiong et al. (2010), and Nemer and Domski (2023). The thermodynamic database DATA0.FM1 contains the Harvie et al. (1984) log K value of Phase 3 (26.0297), and the Xiong et al. (2010) log K value of Phase 5 (42.96), the Nemer and Domski (2023) log K values for Phase 3 (26.33) and Phase 5 (43.81) were input in the EQ3NR input file in the species block as shown below, where the asterisk is used to comment out a line of input. The "commenting out" was appropriately adjusted for each of the four runs shown in Figure 4. Note the example text block below is not from any particular input file, it is simply an illustration of how the log K values were changed.

```
|-------------------------------------------------------------------------------|
|Species                                          |Option          |Alter value |
|  (uxmod(n))                                     |(ukxm(kxmod(n)))|  (xlkmod(n))|
|-------------------------------------------------------------------------------|
|ClO4-                                            |Suppress        | 0.00000E+00|
|H2(aq)                                           |Suppress        | 0.00000E+00|
|O2(aq)                                           |Suppress        | 0.00000E+00|
|Brucite                                          |Suppress        | 0.00000E+00|
|Bischofite                                       |Suppress        | 0.00000E+00|
*|Mg2Cl(OH)3.4H2O                                  |Suppress        | 0.00000E+00|
|Mg2Cl(OH)3.4H2O                                  |Replace         | 26.3300E+00|
|Mg3Cl(OH)5.4H2O                                  |Suppress        | 0.00000E+00|
*|Mg3Cl(OH)5.4H2O                                  |Replace         | 43.8100E+00|
```

The EQ3NR runs were set up using 4.0 m NaCl plus 0.5 m $MgCl_2$ as the starting solution. In EQ6 Mg^{2+} and Cl^- were stoichiometrically titrated into solution as "aqueous species" reactants while either Phase 3 or Phase 5 equilibrium was maintained (see EQ3/6 input description on page 5). Below 0.5 $MgCl_2$ the solubility of Phase 3 and Phase 5 is very high, and it was not possible to maintain equilibrium with those phases which resulted in numerical instability of EQ6. The brucite simulation was carried out in 4.0 m NaCl solution starting at 0.0 m $MgCl_2$ and stoichiometrically titrating Mg^{2+} and Cl^- into solution while maintaining brucite equilibrium. The resulting solution compositions are representative of the simplified GWB and ERDA-6 compositions. The results of the EQ3/6 simulations are presented in Figure 4.

The simulation of results (Figure 4) in the simplified WIPP brine composition (Na-Mg-Cl brine, no carbonate, sulfate, borate, calcium, potassium, iron, or lead) of the Nemer and Domski (2023) log K values for Phase 3 and Phase 5 show that they intersect the brucite stability line at higher Mg concentrations than the values of Harvie and Xiong and are outside the expected Mg compositional range of the WIPP brines. The reacted Mg concentration of GWB and ERDA-6 is ≈ 0.4 m (Domski and Sisk-Scott, 2019), while their initial Mg concentrations are ≈ 1.0 m and ≈ 2 x 10^{-2} m for GWB and ERDA-6, respectively. While the Nemer and Domski (2023) simulations fall outside the expected Mg concentration ranges for GWB and ERDA-6, the Harvie et al. (1984) and Xiong et al. (2010) simulations are in the middle of the GWB range and above the ERDA-6 range. This result is in agreement with the results of Xiong and Lord (2008) who observed Phase 5 in GWB and not in ERDA-6. It must be emphasized that the brine composition used in these simulations is a simplified WIPP composition and is quite different than the expected equilibrium compositions of GWB and ERDA-6 as reported in Domski and Sisk-Scott (2019). None of the experimental studies cited in this memo, neither Xiong and Lord (2008) nor Deng et al. (2009) investigated the occurrence of these phases in brines that are similar to those expected for WIPP conditions. Thus, this modeling exercise illustrates the need for further experimental studies in the Mg

concentration range where Phase 3 and Phase 5 are stable relative to brucite stability in brines expected/predicted by the WIPP baseline solubility model.

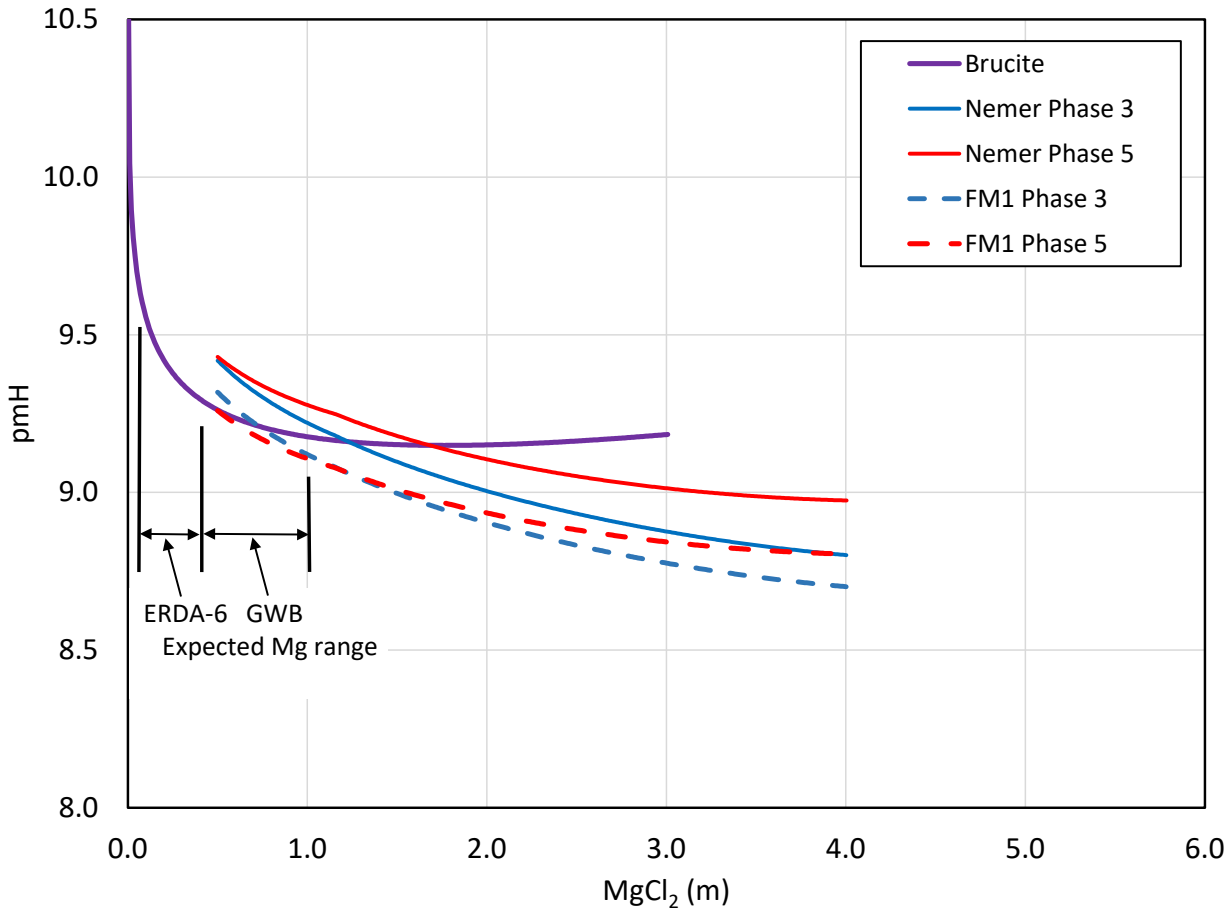

Figure 4. EQ3/6 simulations of brucite, Phase 3, and Phase 5 equilibrium solubility in 4.0 m NaCl titrated with $MgCl_2$. All files stored at: cvs/CVSLIB/WIPP_EXTERNAL_phase5memo.

Summary and Conclusions

The purpose of this memo is to investigate the solubility of Phase 5 and Phase 3 as implemented in the WIPP thermodynamic database, and to gain a better understanding of their mode of occurrence in conditions expected for the WIPP chemical-conditions conceptual model (Wilson et al., 1996).

Altmaier et al. (2003) investigated the solubility and stability of brucite and Phase 3 in NaCl and $MgCl_2$ solutions. Altmaier et al. (2003) calculated the log K values for these phases and found that the values agreed with those of Harvie et al. (1984). Altmaier et al. (2003) performed pre- and post-test phase characterization, as well as during the experiments, using XRD and SEM techniques and found that brucite transformed to Phase 3, and no other magnesium oxychloride phases, most notably Phase 5, were observed. Altmaier et al. (2003) also observed the transformation time of brucite to Phase 3 decreased with increasing $MgCl_2$ solution concentration. It was demonstrated by simulation (Figure 1) that the stability fields for Phase 3 and Phase 5 are very close for the conditions of the Altmaier et al. (2003) experiments, although Altmaier did not observe Phase 5 and may have not tested the Mg concentration where Phase 5 was stable.

Pannach et al. (2017) studied the solubility and occurrence of magnesium oxy-chloride phases in $MgCl_2$ solutions at temperatures ranging from 298 to 393 K. The Pannach et al. (2017) study showed that at 298 K: 1) Brucite was stable in $MgCl_2$ solutions up to 1.5 m before transforming to Phase 3 at 2.0 m (Altmaier saw this transformation at 2.0 m); 2) Phase 5 was observed to form, and forms early in the experiments but is metastable and transforms to Phase 3 over short time frames; and 3) the measured Phase 3 data of Pannach provides support for the WIPP Phase 3 model, as shown in Figure 2, and the need to reexamine the $MgOH^+$ and $MgOH^+/Cl^-$ log β and Pitzer parameters, respectively.

Xiong and Lord (2008) executed a series of experiments to determine the reaction path in the $MgO – CO_2 – H_2O$ system. The only observation that can be made based on this study was that Phase 5 was only observed to form in GWB brine, however, within the uncertainty of the experimental parameters (eg. evaporation) it would be premature to state that Phase 5 formation is exclusive to GWB brine. With absence of measured concentration and pH data it is not possible to determine the conditions under which Phase 5 was observed.

The hydration kinetics of MgO and its hydration products were studied by Deng et al. (2009) who varied the MgO particle size, the solid to brine ratio, and the composition of the brine. The results of this study showed: 1) In GWB the hydration products of periclase follow the reaction path of Phase 5 followed by brucite precipitation; 2) periclase hydration in simplified GWB is rapid and more complete than observed in the full GWB composition brine; and 3) the simulated solubility using the log K value of Xiong et al. (2009) underpredicts the measured Phase 5 solubility. However, this last result is questionable given the mixed nature of the solid phases in solution, and the uncertainty of which phase is controlling Mg solubility.

Xiong et al. (2010) investigated the solubility of Phase 5 in the $Na – Mg – Cl – H_2O$ system at varying concentrations. They calculated the log K value of Phase 5 for the SIT aqueous model (43.21 ± 0.33), and the Pitzer model (42.96 ± 0.32). The log K value was shown (Figures 4 and 5) to underestimate the measured Phase 5 solubility data. The final phase assemblage in the Xiong et al. (2010) experiments was not discussed, therefore, it may be possible that secondary phases, such as hydromagnesite, may have formed which could influence the measured data and the calculated log K value.

Based on this literature survey of the magnesium oxy-chloride phases, and the comparison of the literature experimental data to the simulated behavior of Phase 3 and Phase 5 it can be argued that Phase 3 and Phase 5 phase stabilities appear to be very close, and that the occurrence of Phase 5 requires further study for WIPP repository conditions. Both Altmaier et al. (2003) and Pannach et al. (2017) examined the same compositional space in their studies, and Altmaier did not observe Phase 5, while Pannach did observe it, but as a metastable phase which converted to Phase 3. In their review of magnesium oxy-chloride cements Urwongse and Sorrell (1980), Guo et al. (2018), and Tan et al. (2021) note the metastable nature of Phase 5 and subsequent conversion to Phase 3 in cement pastes.

The solubility of Phase 3 and Phase 5 implemented in the WIPP model was compared to the measured data of the studies using EQ3/6 and the DATA0.FM1 database[5]. The model fits are presented in Figure 1 and Figure 2 and subjectively the model appears to fit the measured Phase 3 data relatively well. The model fit to the measured Phase 5 data consistently underestimates its solubility (Figure 3). The model fits also show that the stability fields for Phase 3 and Phase 5 are very close which is to be expected based on the observation that Phase 5 is metastable and converts to Phase 3 (Figure 4).

[5] The log K values and associated Pitzer parameters for Phase 3 and Phase5 have not changed since they were added to the DATA0.FM1 and have not changed in the current QA database DATA0.FM5 (Domski, 2020).

In conclusion, based on these observations, and the uncertainty in the solubility of these phases (Nemer and Domski, 2023) as shown in Figure 4, it is recommended that for future recertification analyses, or until new experimental evidence and thermodynamic parameters become available (i.e., the DATA0.FM1 $Mg(OH)_2 – MgCl_2 – H_2O$ model is updated), Phase 5 should be suppressed from forming in the baseline actinide solubility model.

References

Altmaier, M., V. Metz, V. Neck, R. Muller, T. Fanghanel. (2003). "*Solid-liquid equilibria of $Mg(OH)_2$(cr) and $Mg_2(OH)_3Cl{\cdot}4H_2O$(cr) in the system Mg-Na-H-OH-O-Cl-H2O at 25 °C"*. Geochem. Cosmochim. Acta 67 3595–3601.

Brush, L.H., P.S. Domski, and Y.-L. Xiong. 2012. "Analysis Plan for WIPP Near-Field Geochemical Process Modeling." AP-153, Rev. 1, February 8, 2012. Carlsbad, NM: Sandia National Laboratories. ERMS 556960.

Deng, H., Y. Xiong, M. Nemer, and S. Johnsen. 2009. Experimental Work Conducted on MgO Long-Term Hydration, Milestone Report. Carlsbad, NM: Sandia National Laboratories. ERMS 551421.

Domski, P. and C. Sisk-Scott. 2019. Prediction of Baseline Actinide Solubilities for CRA 2019 with and Updated EQ3/6 Pitzer Thermodynamic Database, DATA0.FM4. Carlsbad, NM: Sandia National Laboratories. ERMS 571178

Domski, P.S. 2020. DATA0.FM5: Official Release of the Qualified Pitzer Thermodynamic Database, DATA0.FM5, for EQ3/6 under AP-183, Revision 1. Carlsbad, NM: Sandia National Laboratories. ERMS 572791

Guo, Y., Y. Zhang, K. Soe, M. Pulham. (2018). Recent development in magnesium oxychloride cement. Structural Concrete. DOI: 10.1002/suco.201800077. 2018;19:1290–1300.

Mazuranic, C., H. Bilinski, B. Matkovic, *"Reaction-products in the system $MgCl_2$-NaOH-H_2O*". J. Am. Ceram. Soc. 65 (1982) 523–526.

Nemer. M. and P. Domski, 2023. Bayesian Inference applied to the Solubility of Phase-3 and Phase-5. Carlsbad, NM: Sandia National Laboratories. ERMS pending.

Pannach M, Bette S, Freyer D. "*Solubility Equilibria in the system $Mg(OH)_2$-$MgCl_2$-H_2O from 298 to 393°K"*. Journal Chem Eng Data. 2017;62(4):1384–1396.

Peake, T. 2022. Letter to Michael Gerle "CRA-2019 Issues Table". U.S. Environmental Protection Agency, Center for Waste Management and Regulations. June 30, 2022.

Tan, Y., W. Chengyou, Y. Hongfa,L. Ying, W. Jing. (2021). "Review of reactive magnesia-based cementitious materials: Current developments and potential applicability". Journal of Building Engineering. Volume 40, August 2021, 102342.

Urwongse L, Sorrell CA. "*The system MgO-$MgCl_2$-H_2O at 23°C"*. Journal American Ceramic Soc. 1980;63(9–10):501–504.

U.S. EPA. 2022. "Technical Support Document for Section 194.24: "*Evaluation Of The Compliance Recertification Application (Cra-2019) Actinide Source Term, Gas Generation, Backfill Efficacy, Water Balance, And Culebra Dolomite Distribution Coefficient Values*" EPA Docket: EPA-HQ-OAR-2019-0534. Washington, DC: U.S. Environmental Protection Agency Office of Air and Radiation.

Wilson, C., D. Porter, J. Gibbons, E. Oswald, G. Sjoblom, and F. Caporuscio. 1996a. *Final Waste Isolation Pilot Plant Conceptual Models Report*. July 1996. Carlsbad, NM: U.S. Department of Energy Carlsbad Area Office.

Xiong Y.-L. and Lord A. S. (2008). "*Experimental investigations of the reaction path in the MgO–CO_2–H_2O system in solutions with various ionic strengths, and their applications to nuclear waste isolation*." Appl. Geochem. 23, 1634–1659.

Xiong, Y.-L., H.-R. Deng, M.B. Nemer, and S. Johnsen. (2009). "*Thermodynamic Data for Phase 5 ($Mg_3Cl(OH)_5{\cdot}4H_2O$) Determined from Solubility Experiments*". Memorandum to L.H. Brush, May 18, 2009. Carlsbad, NM: Sandia National Laboratories. ERMS 551294.

Xiong, Y.-L. H.R. Deng, M. Nemer. (2010). "*Experimental determination of the solubility constant for magnesium chloride hydroxide hydrate ($Mg_3Cl(OH)_5{\cdot}4H_2O$, phase 5) at room temperature, and its importance to nuclear waste isolation in geological repositories in salt formations"*. Geochem. Cosmochim. Acta 74 (2010) 4605–4611.

Xiong, Y.-L. (2011). "*Release of EQ3/6 Database DATA0.FM1*." E-mail to Jennifer Long, March 9, 2011. Carlsbad, NM: Sandia National Laboratories. ERMS 555152.

APPENDIX A:

Table A-1: Xiong and Lord (2008) Experimental Matrix

Experimental Conditions						
Figure	**Solution Composition**	**pCO_2**	**Solid Reactant**	**Condition**	**CO_2 Condition**	**Products**
1	DI Water	-3.4	P MgO	Static	Passive	H B C P
2	4.4 m NaCl	-3.4	P MgO	Static	Passive	B C HA P
3	ERDA-6	-3.4	P MgO	Static	Passive	B C HA P
4	GWB	-3.4	P MgO	Static	Passive	MC B C HA P
5	4.4 m NaCl	-3.4	P MgO	Stirred	bubbled	H C P
5	DI Water	-3.4	P MgO	Stirred	bubbled	H C P
5	ERDA-6	-3.4	P MgO	Stirred	bubbled	H C P
5	GWB	-3.4	P MgO	Stirred	bubbled	H C P
7	0.010 m NaCl	-3.4	F Mg(OH)2	Static	Passive	H B
8	0.10 m NaCl	-3.4	F Mg(OH)2	Static	Passive	H B
9	1.0 m NaCl	-3.4	F Mg(OH)2	Static	Passive	H B
10	4.4 m NaCl	-3.4	F Mg(OH)2	Static	Passive	H B HA
11	ERDA-6	-3.4	F Mg(OH)2	Static	Passive	H B HA
12	GWB	-3.4	F Mg(OH)2	Static	Passive	MC H B HA
13	ERDA-6	-1.3	F MgO	Stirred	bubbled	N H B HA
14	GWB	-1.3	F MgO	Stirred	bubbled	H B HA
15	ERDA-6	-1.3	ph F MgO	Stirred	bubbled	N H B HA
16	GWB	-1.3	ph F MgO	Stirred	bubbled	H B A
6a	DI Water	-3.4	F Mg(OH)2	Stirred	bubbled	H B
6b	DI Water	-3.4	F Mg(OH)2	Static	Passive	H B

Abbreviations:

P MgO = Premeir MgO
F MgO = Fisher MgO
F MgO = Fisher MgO
ph F MgO = prehydrated Fisher MgO

H = hydromagnesite
B = brucite
C = calcite
P = periclase (MgO)
HA = halite
MC = Mg-Oxy-Chloride (phase 5)
N = nesquehonite
A = anhydrite

Table A-2. Xiong et al. (2010) experimental matrix.

Designation	**NaCl (m)**	**$MgCl_2$ (m)**
$MgCl_2$-A	5.0	0.5
$MgCl_2$-B	3.5	0.8
$MgCl_2$-C	3.0	1.3
$MgCl_2$-D	2.0	1.5
$MgCl_2$-E	1.5	1.8
$MgCl_2$-F	0.5	2.0